Air–Water Interface Jetting Induced by Explosion Load

Guifu Zhang, Yujian Zhu, and Jiming Yang

Introduction

Explosion in liquid emits a shock wave and induces a radial flow with a bubble in center. When it occurs near a free surface, a jet may develop. The effect can be enhanced by restricting the flow only to the jetting direction, e.g., in a tube container. The jet is seen as a potential tool for mass delivery and material breaking. Specific applications of it require solid understanding of the underlying jetting dynamics.

The dynamic causes of interfacial jetting are manifold, among which the interaction of in-liquid explosion with free surface is a major one. Early experimental and theoretical works of Chahine, Blake, and Gibson et al. [1–3] established the fundamental knowledge on this process. By numerical simulation, Wang [4] analyzed the possible influence of buoyancy, and Liu [5] looked into the transient shock-interface interaction process shortly after the explosion. Dadvand et al. [6] examined the role of an orifice plate placed on the free surface in suppressing the satellite droplets and reshaping the main jet. Zhang et al. [7] carried out a systematic investigation on the bubble and jetting phenomenon caused by an explosion between parallel free surface and rigid wall.

The phenomenon becomes even complicated when it occurs in a tube container. Exact investigations targeting this phenomenon are relatively rare. Ohki et al. showed that the jet velocity increases linearly with the energy of laser pulse while it first increases and then decreases with the standoff distance. Similar experimental investigation was conducted by Tagawa et al. [8]; based on which, an empirical law correlates the jet velocity with the explosion energy, the standoff distance, the tube diameter, and the contact angle of free surface which was proposed. They proceeded with numerical simulations and a more complete discussion on the law of jet velocity [9].

In this study, we investigate the air–water interface jetting induced by an explosion in a straight round tube, experimentally. The scale of present phenomenon is much larger than that of Tagawa and Peters [8, 9], and the influence of interface curvature is out of our consideration. Electrical wire explosion is applied. Direct high-speed photography is employed to diagnose the flow. The effects of discharging energy (voltage), explosion depth, and tube diameter on the flow pattern and the jet velocity are examined.

Experimental Setup

Figure 1 shows the main experimental setup of this study. Electric spark method is applied to generate the explosion. The drive circuit (Fig. 1a) includes a DC power, a set of capacitors which add up to 500 μF, and a SPDT relay to switch between charge and discharge states. The explosion energy is tuned by varying the charging voltage. The total electrical energy discharged then can be estimated by $E = \frac{1}{2}CU^2$. The exploding wire, which is of nichrome, 0.05 mm in diameter and 1 mm in length, is installed on the electrodes on the tube bottom. Four different tube diameters, $D = 10, 13, 22, 32$ mm, are tested.

The main diagnostic technique is direct photography of the flow followed by digital processing and measurement of the obtained images. A high-speed video camera is employed to capture the quick interfacial phenomena. Speed of the camera for current study is mostly set to 2000 fps.

G. Zhang (✉) • Y. Zhu • J. Yang
Department of Modern Mechanics, University of Science and Technology of China, Hefei, Anhui 230027, China
e-mail: zgfu@mail.ustc.edu.cn
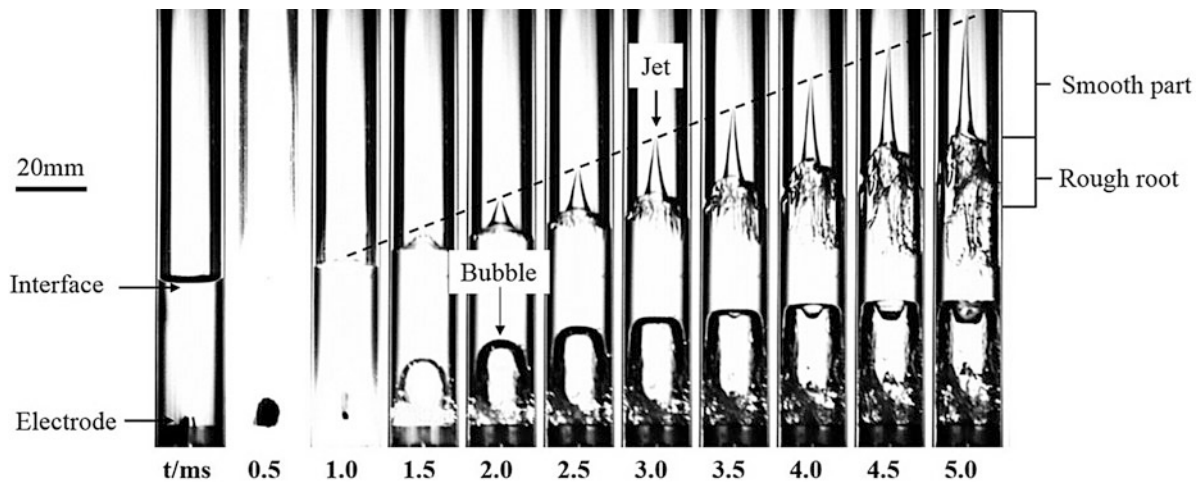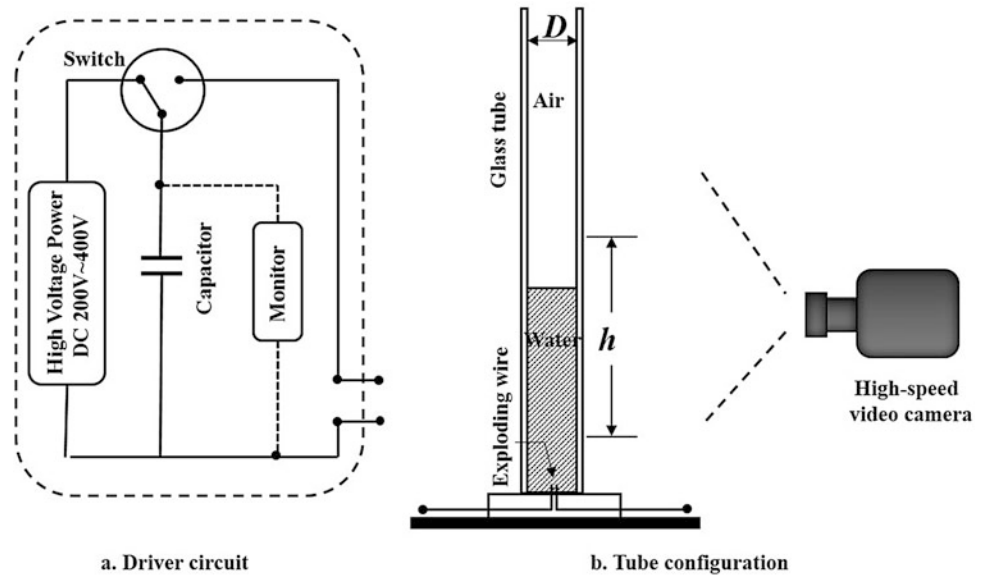
Fig. 1 Schematic of
experimental setup

a. Driver circuit   b. Tube configuration

Fig. 2 Sequential images of interfacial flow in a straight tube, $D = 13$ mm, $U = 350$ V, $C = 500$ μF, $h = 40$ mm

Results

Patterns of Jetting Flow

By varying the tube diameters D, charging voltage U, and explosion depths h, the jetting flow exhibits different patterns. For small tube diameters, $D = 10$ and 13 mm, the jet appears to be the commonly spiky shape with a sharp end; for large tube diameters, $D = 22$ and 32 mm, other unusual jet patterns are observed—typically the bowl shape and the combined bowl and stamen shape.

Sharp Jet

The development of the spiky jet as well as the accompanying bubble dynamics is shown in Fig. 2.

Corresponding test conditions are $D = 13$ mm, $h = 40$ mm, and $U = 350$ V.

The air–water interface can be seen clearly in the first frame ($t = 0$ ms), as are the two tiny electrodes where the explosion and the bubble will emerge. At the initial stage of the explosion, the nichrome wire vaporizes and ionizes producing an extremely high-temperature plasma bubble. This hot and luminous bubble can be seen in the second and third frames. The bubble appears hemisphere in the first place, and then the horizontal explosion ceases due to the confinement of the tube walls, whereas vertical explosion still goes on. Along with the bubble, growth pressure and temperature in bubble keep decreasing. As being over-expanded, the bubble starts to collapse from its upper wall as shown in the eighth frame (3.5 ms) of Fig. 2.

0.5–1.0 ms after the explosion, the water surface lifts and focuses to a jet. In this process, a cavitation region develops

at the joint of sidewall and free surface which penetrates downward and form a rough interface because of Rayleigh–Taylor instability (3.0–5.0 ms). Thus, the surface jet is clearly divided into two distinct parts—a smooth upper body and a rough root. The structure features the jet in a tube and differs from that in fully open environment.

By processing and measurement of the images, it is also found that the surface jet rises almost at a constant velocity (Fig. 2, vertical positions linearly increases with time).

Bowl-Shaped Jet

The bowl-shaped jet merges generally in case of large tube diameter. Typical developing process of the jet is shown in Fig. 3, where $D = 32$ mm, $U = 400$ V, and $h = 40$ mm.

The bubble evolution is essentially the same as that of the previous case, except that here the bubble is relatively small comparing to the size of tube. The surface jet however undergoes a different evolution. The surface lifts with the expansion of bubble, which then turns into a flat platform. Baroclinic effect due to interaction of shock and capillary-induced surface curvature counts for the initial detachment of platform from the tube wall. The platform converges very slowly and fails to gather into a sharp jet eventually. When the bubble switches to collapse phase ($t = 3.0$ mm), the rim of the platform seems to be unaffected by the contraction of bubble, while the central part of the platform is clearly obstructed by the pressure difference between atmosphere and bubble. This brings to a bowl-shaped jet as that in frames of 3.5 mm thereafter.

Bowl and Stamen Jet

A special bowl-shaped jet may form as the explosion depth is small enough. That is a sharp jet emerges from the center of a bowl or platform. We call this type of jet blow and stamen jet. Typical flow patterns of the jet are shown in Fig. 4, where $D = 32$ mm, $U = 400$ V, and $h = 10$ mm. Because the explosion depth is small relative to the tube radius or the maximum bubble radius, the bubble expand very fast and the roof of bubble overtops the average air–water interface within 1 ms after the explosion. This leads to a quick hump-up of the free surface which is the origin of the stamen jet. On the other hand, the overall water column above the bubble lifts and detaches from the tube wall, under a similar mechanism as that of the bowl-shaped jet. Overlap of the two forms the so-called bowl and stamen jet.

Velocity of Jetting Flow

By image processing, the velocity of jet can be measured. The distribution of jet velocity versus explosion depth and charging voltage in different diameter of tubes is shown in Fig. 5 (scatters). It is obvious that the jet velocity increases with the U but decreases with h and D.

A 1D theoretical model is established to analyze the jet velocity and its dependence. The process is approached with the motion of a water piston driven by a compressible gas column. Deformation of the water is not considered. The gas is assumed calorically perfect, and the expansion and
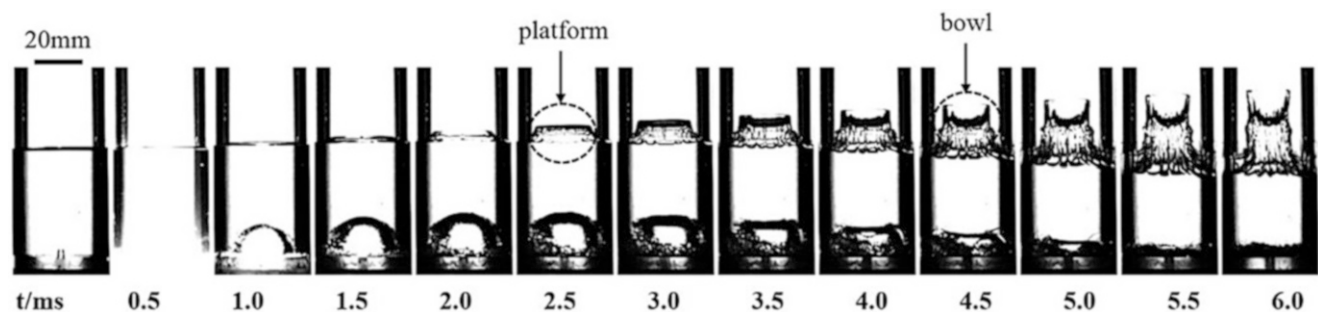

Fig. 3 Sequential images of interfacial flow in a straight tube, $D = 32$ mm, $U = 400$ V, $C = 500$ μF, $h = 40$ mm
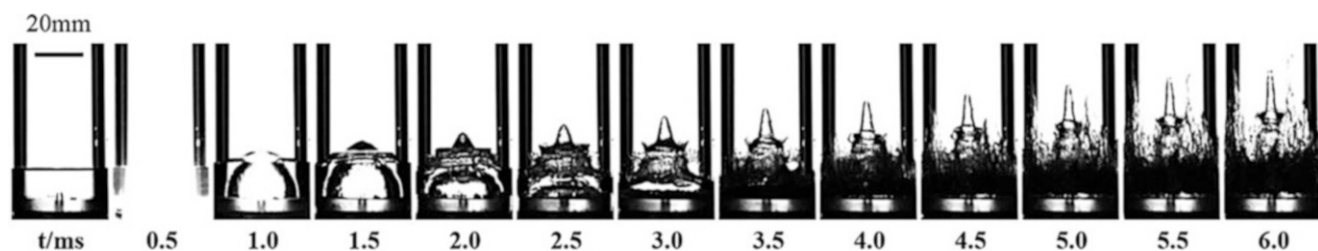

Fig. 4 Sequential images of interfacial flow in a straight tube, $D = 32$ mm, $U = 400$ V, $C = 500$ μF, $h = 10$ mm
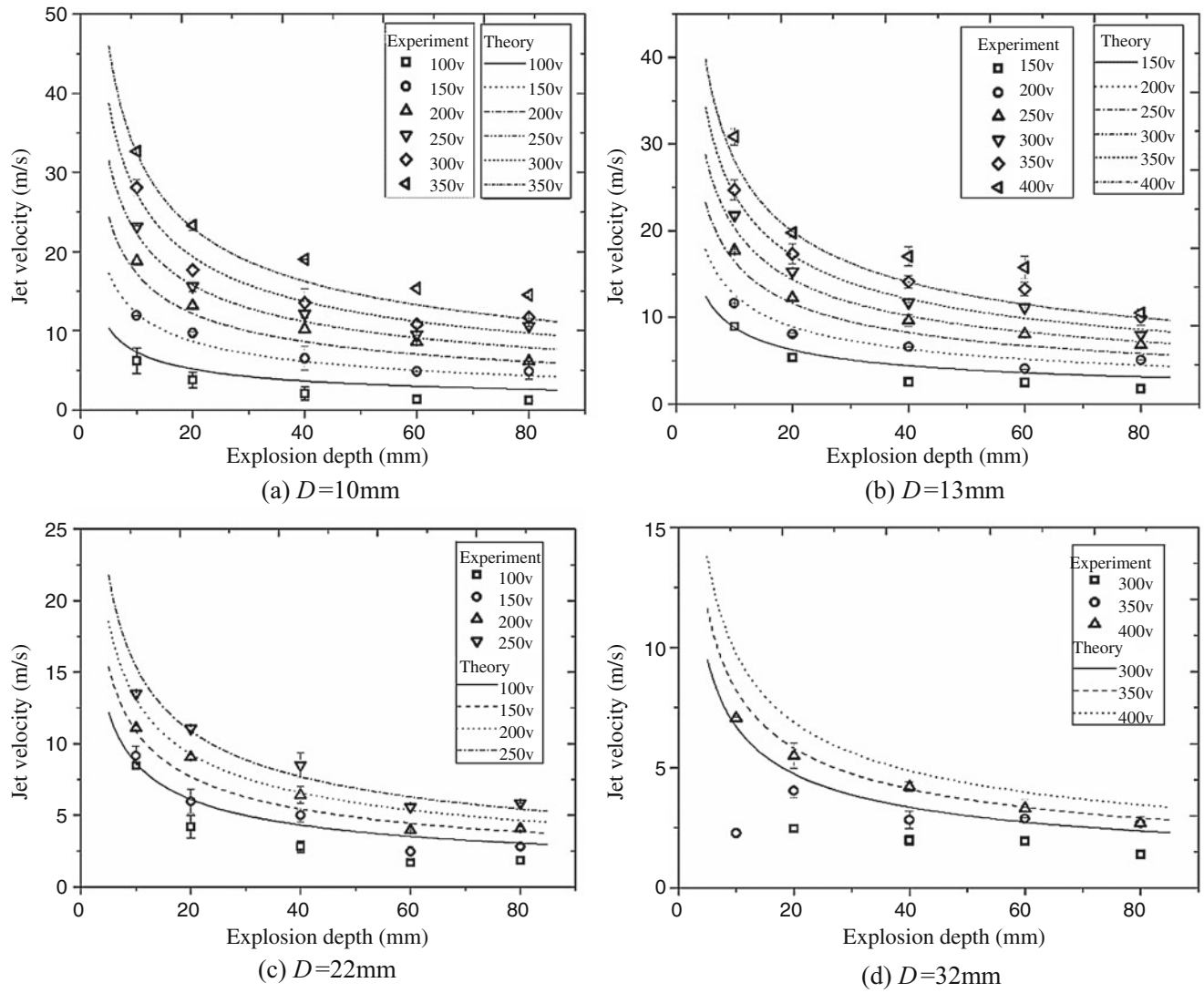
Fig. 5 Variation of surface jet velocity

compression of it are spatially uniform, adiabatic, and isentropic. Applying Newton's second law and ignoring the friction, we have

$$
\begin{cases}
\dfrac{\mathrm{d}^2 L}{\mathrm{d}t^2} = \left(\dfrac{L_0}{L}\right)^\gamma \cdot \dfrac{P_{b0}}{\rho_w \cdot h} - \dfrac{P_a}{\rho_w \cdot h} \\
\text{I.C.:} \quad t = 0, L = L_0, \dfrac{\mathrm{d}L}{\mathrm{d}t} = 0
\end{cases}
\tag{1}
$$

where h is the thickness of water column (explosion depth), ρ_w is the density of water, L is the thickness of the gas column and P_b is the pressure of it, L_0 and P_{b0} stand for the initial values of L and P_b, $P_a = 1\,\mathrm{atm}$ is the constant ambient pressure, and γ is the specific heat ratio which takes 1.4 for the current study.

Providing L_0 and P_{b0}, the motion of water piston can be solved as a function of time. Two characteristic parameters

are picked up for the analysis. One is the maximum gas volume which for a given tube diameter is solely determined by L_{max}, and the other is the maximum piston velocity $v_{max} = (\mathrm{d}L/\mathrm{d}t)_{max}$. It is found that, by assigning L_0 and P_{b0} so that the maximum gas volume matches experimental bubble volume, the resulted maximum piston velocity will approximate the real jet velocity. We then choose one reference case to get a proper L_0^{ref} and P_{b0}^{ref}.

The other cases take the same $L_0 = L_0^{ref}$ while calculating P_{b0} by

$$
P_{b0} = \left(\frac{U \cdot D^{ref}}{U^{ref} \cdot D}\right)^2 \cdot P_{b0}^{ref}
\tag{2}
$$

to take into account the influence of tube diameter D as well as the charging voltage U. Figure 5 (lines) shows the

computational results. It turns out for majority of the cases, not only the variation trend but also the exact value of jet velocity can be well predicted by this model. Deviation becomes more evident though when the tube diameter is large, e.g., $D = 32$ mm, where the computational results are generally higher than the experimental measurements. This is simply because the 1D approach goes invalid as the bubble is comparably small to the tube diameter.

The agreement between the theoretical maximum piston velocity and the experimentally measured jet velocity also indicates that the jet gains its velocity as a part of the entire lifting column at the very beginning of the bubble expansion. The projecting part of the jet maintains this velocity, while the rest part is obstructed due to reversed pressure action.

Conclusions

The air–water interfacial jetting flows in tubes induced by underwater explosion under varied conditions are investigated experimentally. Direct high-speed photography is employed to record the interfacial flow patterns as well as to provide flow information for further analysis. Different tube diameter, explosion depth, and energy are tested.

It is found that the common sharp jet appears in cases of small tube diameter and bowl-shaped jet appears when the tube diameter is relatively large to the bubble size. There is also a special jet pattern that combines the platform/bowl jet and a sharp stamen jet in center, as the tube is large and the explosion is shallow.

A quasi-1D theoretical model is established to study the dependence of jet velocity on test conditions. It presents good agreement between the experimental data and theoretical calculations except when the tube diameter is too large that violates the 1D assumption. The agreement also indicates that the jet gains its velocity as a part of the lifting column at the beginning of the explosion.

References

1. Chahine, G.L.: Interaction between an oscillating bubble and a free surface. Trans. ASME: J. Fluid Eng. **99**, 709–716 (1977)
2. Blake, J.R., Gibson, D.C.: Cavitation bubbles near boundaries. Annu. Rev. Fluid Mech. **19**, 99–123 (1987)
3. Blake, J.R., Taib, B.B., et al.: Transient cavities near boundaries: free surface. J. Fluid Mech. **181**, 197–212 (1987)
4. Wang, Q.X., Yeo, K.S., et al.: Nonlinear interaction between gas bubble and free surface. Comput. Fluids **25**(7), 607–628 (1996)
5. Liu, T.G., Khoo, B.C., et al.: The simulation of compressible multi medium flow: II. Applications to 2D underwater shock refraction. Comput. Fluids **30**, 315–337 (2001)
6. Dadvand, A., Khoo, B.C., et al.: A collapsing bubble induced micro injector: an experimental study. Exp. Fluids **46**, 419–434 (2009)
7. Zhang, A.M., Cui, P., et al.: Experiments on bubble dynamics between a free surface and a rigid wall. Exp. Fluids **54**, 1602 (2013)
8. Tagawa, Y., Oudalov, N., van der Meer, D., Sun, C., Prosperetti, A., Lohse, D., et al.: Highly focused supersonic microjets. Phys. Rev. X **2**, 031002 (2012)
9. Peters, I.R., Tagawa, Y., van der Meer, D., et al.: Highly focused supersonic microjets: numerical simulations. J. Fluid Mech. **719**, 587–605 (2013)